Near Infrared Laser–Annealed IZO Flexible Device as a Sensitive H_2S Sensor at Room Temperature

Po-Yi Chang[1,2,3], Ching-Fu Lin[1,2,3], Samer El Khoury Rouphael[2,3],Ting-Hsuan Huang[1], Chang-Mao Wu[1], Dominique Berling[2,3], Ping-Hung Yeh[4], Chia-Jung Lu[5], Hsin-Fei Meng[6], Hsiao-Wen Zan[1*], Olivier Soppera[2,3*]

[1.] *Department of Photonics and Institute of Electro-Optical Engineering, National Chiao Tung University, 1001 Ta Hsueh Rd. Hsinchu, Taiwan.*

[2.] *Université de Haute-Alsace, CNRS, IS2M UMR 7361, F-68100 Mulhouse, France*

[3.] *Université de Strasbourg, France*

[4.] *Department of Physics, Tamkang University, No.151, Yingzhuan Rd., Tamsui Dist., New Taipei City, 25137, Taiwan*

[5.] *Department of Chemistry, National Taiwan Normal University, 162, Section 1, Heping E. Rd., Taipei, Taiwan*

[6]*Institute of Physics, National Chiao Tung University, 1001 Ta Hsueh Rd. Hsinchu, Taiwan.*

E-mail: hsiaowen@mail.nctu.edu.tw , olivier.soppera@uha.fr

Keywords :

gas sensor, IZO, sol-gel, laser annealing, NIR, flexible

Abstract

A metal-oxide material (indium zinc oxide [IZO]) device with near-infrared (NIR) laser annealing was demonstrated on both glass and bendable plastic substrates (polycarbonate, polyethylene, and polyethylene terephthalate). After only 60 s, the sheet resistance of IZO films annealed with a laser was comparable to that of thermal-annealed devices at temperatures in the range of 200°C–300°C (1 hr). XPS, ATR, and AFM were used to investigate the changes in the sheet resistance and correlate them to the composition and morphology of the thin film. Finally, the NIR laser-annealed IZO films were demonstrated to be capable of detecting changes in humidity and serving as a highly sensitive gas sensor of hydrogen sulfide (in parts-per-billion concentration), with room-temperature operation on a bendable substrate.

Introduction

In recent years, with the emergence of the Internet of Things, the development of various types of sensors has become increasingly critical. Gas sensors in particular have drawn much attention because of their ability to give an alert in the presence of toxic or explosive gas for safety surveillance,[1] monitor air pollution conditions,[2]

detect health conditions through analysis of human breath,[3-6] and control the freshness of food stock.[7,8] Incorporating solid-state semiconductor gas sensors into plastic parts or wearable devices has also become attractive to facilitate easy handling and real-time detection.[9,10]

Metal-oxide semiconductor materials grown through a conventional vacuum process have been successfully used in many commercial gas detectors.[9,11,12] However, complex and expensive equipment and high-temperature operation are usually required in the fabrication of such sensors.[10,13,14] Along with the development of low-cost solution-processed metal-oxide semiconductor devices, many researchers have aimed to use a solution process to produce gas sensors on flexible or even stretchable substrates. For this, the operating temperature must be lower to preserve the properties of the plastic substrate. Room-temperature operation is still a challenging but attractive characteristic of the sensors. Myoung et al. developed micropatternable zinc oxide nanoflowers on polyimide substrate to detect nitrogen dioxide at 270°C (operating temperature).[15] Xu and team developed a special metal-organic coating and applied it on ZnO nanowires to realize a sensitive acetone sensor at 260°C.[12] Zheng et al. used commercial ZnO nanoparticles together with an ultraviolet (UV)-light-controlling technique to form an ethanol sensor on a polyethylene terephthalate (PET) substrate at room temperature.[16] Li et al. used an in

situ chemical oxidation polymerization method to prepare polyaniline, a flower-like WO_3 nanocomposite, on a PET substrate to detect 500-ppb ammonia at room temperature.[17] Our previous work involved applying polymer-coating layers onto sputtered Indium-Gallium-Zinc-Oxide (IGZO) thin-film transistors to perform room-temperature ammonia and acetone sensing.[18] Most successful metal-oxide-based gas sensors on flexible substrates exhibit nanostructures in their active layer. Few reports have demonstrated successful gas-sensing performance with the use of a solution-processed metal-oxide thin film. Jaisutti et al. reported the production of a sol–gel IGZO thin film on a glass substrate for detecting acetone at room temperature under UV irradiation.[19] The photochemically activated IGZO film did not require a thermal-annealing process; thus, it may also be applicable to flexible substrates.

For fabricating sensors on flexible substrates, the low curing temperature was also required. In prior studies including our prior reports, the decrease in the curing temperature relied on the use of UV treatment on metal-oxide sol–gel precursors. Such conditions proved to be very effective in removing the organic ligands and cross-linking the material.[20-24] However, use of them is usually not sufficient for obtaining enough formation of a metal-oxide inorganic network with suitable electrical properties. In particular, the defect level is too high before thermal

treatment.[21] For this reason, we decided to investigate near-infrared (NIR) laser curing.

NIR laser curing was introduced as an efficient technique with which to induce photothermal effects in materials absorbing the NIR. This effect has already been used in applications such as laser marking,[25-27] polymer melting for particle migration,[28] and polymer-to-polymer fixation. In this work, we demonstrate that NIR laser irradiation can be used for curing metal-oxide precursor thin films prepared from solutions, with sol–gel chemistry. The NIR laser system with a wavelength of 808 nm and continuous irradiation was used to irradiate a sol–gel IZO xerogel thin film to activate its electrical property. In addition to the electrical characterization, material analysis methods such as X-ray photoelectron spectroscopy (XPS) and attenuated total reflection Fourier-transform infrared spectroscopy (ATR-FTIR) were used to investigate the NIR-laser-annealed IZO film. The low temperature process made it possible to integrate the IZO thin film onto the flexible polymer substrates of polycarbonate (PC), polyethylene (PE), and PET. Last, we determined that the IZO film can act as a gas sensor. The electrical properties were modified according to the presence of water in the atmosphere, allowing the use of the device as a humidity sensor. With a fixed humidity control, the IZO film also detected hydrogen sulfide gas down to 300 parts-per-billion (ppb) concentration at room temperature. Compared

with prior works demonstrating flexible hydrogen sulfide sensors,[29-31] we are the first to realize the ppb-regime sensitivity on a flexible substrate, revealing its potential for application in wearable devices. According to the recommendation of the American Conference of Governmental Industrial Hygienists, the long-term (8 h time-weighted average) exposure limit for hydrogen sulfide is 1 ppm. The developed ppb-regime detection capacity is beneficial for the early alert of a dangerous environment. In this study, our proposed hydrogen sulfide sensor was sensitive, fast, and reversible, indicating promising applications in environmental surveillance.

Experimental

[Device fabrication]

Figure 1a shows the schematic of device fabrication. The devices were produced using 3 cm × 3 cm substrates, which can be either glass or flexible plastic materials such as PC, PE, or PET with 0.2-mm thickness. After cleaning the substrate, we used 10-mins oxygen plasma (in a reactive ion etching system) at 100 W on glass substrates or 20-mins UV ozone treatment (Orient Service Co. Ltd; TW-UN-URS-500-03) on plastic substrates to produce hydrophilic surfaces to facilitate the following film adhesion. Then, the IZO precursor solution was spin-coated on the glass substrate. Here, we used indium(III) nitrate hydrate [$In(NO_3)_3 \cdot xH_2O$] and zinc nitrate hydrate [$Zn(NO_3)_2 \cdot xH_2O$] precursors (both

purchased from Sigma-Aldrich) dissolved in 2-methoxyethanol (In:Zn=5:4, [In]+[Zn]=0.25 M). Because the sol–gel solution and thin films are transparent at 808 nm, a dye was added to the IZO solution. IR-140 (Sigma-Aldrich) was chosen for its solubility in the solution (typ. 1.2 wt%) and strong absorption at the NIR laser wavelength (Figure S1). IR-140 acts as a photoabsorber, provoking a photothermal effect in the sol–gel film, which was proved to be necessary to guarantee the stability of device performance. The absorption of the substrates was low at 808 nm as shown in Fig. S2 in supporting information, and thus no visible effect of the laser irradiation was observed on raw substrates in the range of power used here. This approach thus allowed thermal curing of the sol–gel layer without substantially affecting the properties of the substrate, which is the objective of this work.

After the coating process, the laser annealing treatment was applied (Figure 2b). The irradiation area was 5×5 mm^2 (Figure 2c) using an NIR 808 nm continuous laser (DS3-11312-xxx-LD No., BWT Beijing). The distance between the laser head and the sample is 15 cm. After laser annealing, the substrate was baked at 50°C for 20 min. The thickness for IZO film after annealing was about 100 nm, confirmed by ET200 (SANPANY INSTRUMENTS CO., LTD.). Finally, the aluminum electrodes (60 nm) were deposited by thermal evaporation to form an IZO chemoresistor. The spacing between the two electrodes was 200 μm.

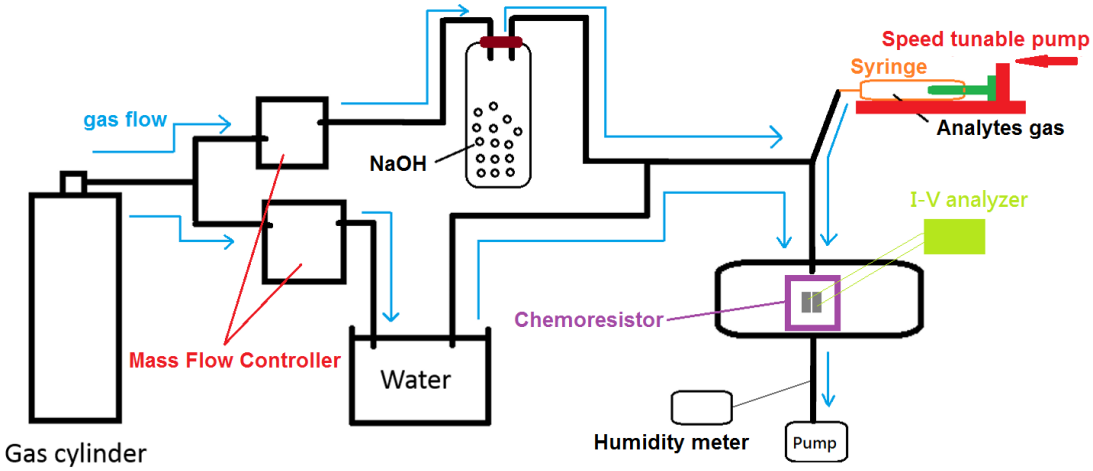

Figure 1. The schematic diagram for the sensing system.

The humidity detection system, as shown in Figure 1, delivered an air flow with a tunable relative humidity (RH). The RH was controlled by tuning the flow ratio between the "dry air" and the "wet air" settings, where the dry air is the ambient air passing through a NaOH tube to exhibit a RH of approximately 10% and the wet air is the ambient air passing through a bottle of water to deliver a RH of approximately 80%. To adjust the final RH, the flow rates of the dry and wet air were controlled by flow meters. With a pump in the outlet of the system, the mixed air with an adjustable RH was then injected into a glass tube, which served as the sensing chamber with the IZO chemoresistor.

For hydrogen sulfide (H_2S) gas detection, as shown in Figure 1, the background air (with an RH set at approximately 62% by the aforementioned humidity system) was pumped into the sensing chamber at a flow rate of 500 mL/min to serve as the

carrier gas. The analyte gas such as H_2S gas was injected into the system to mix with the background air through a syringe pump system. Inside the syringe, 100-ppm H_2S was placed. By tuning the speed of the syringe pump, the concentration of H_2S in the mixed gas ranged from 300 to 1000 ppb. Inside the sensing chamber, the device current was recorded along with time by using an I-V analyzer (Agilent U2722A).

The XPS analysis was performed on two setups: a Gammadata Scienta (Uppsala, Sweden) SES 200-2 X-ray photoelectron spectrometer under ultrahigh vacuum conditions ($P < 10^{-7}$ Pa) to collect thermal annealing data and on a PHI Quanterall, ULVAC-PHI ($P < 2.0 \times 10^{-7}$ Pa) to collect NIR laser annealing data, separately. CASAXPS (Casa Software Ltd, Teignmouth, UK, www.casaxps.com) was used to fit all the peaks and area of each component of XPS data. ATR spectra were acquired using an IS50 spectrophotometer from Thermo Scientific. Diamond was supplied by Specac (Golden Gate diamond, with a 45° angle). Film roughness was characterized using AFM in tapping mode (Picoplus system from Agilent).

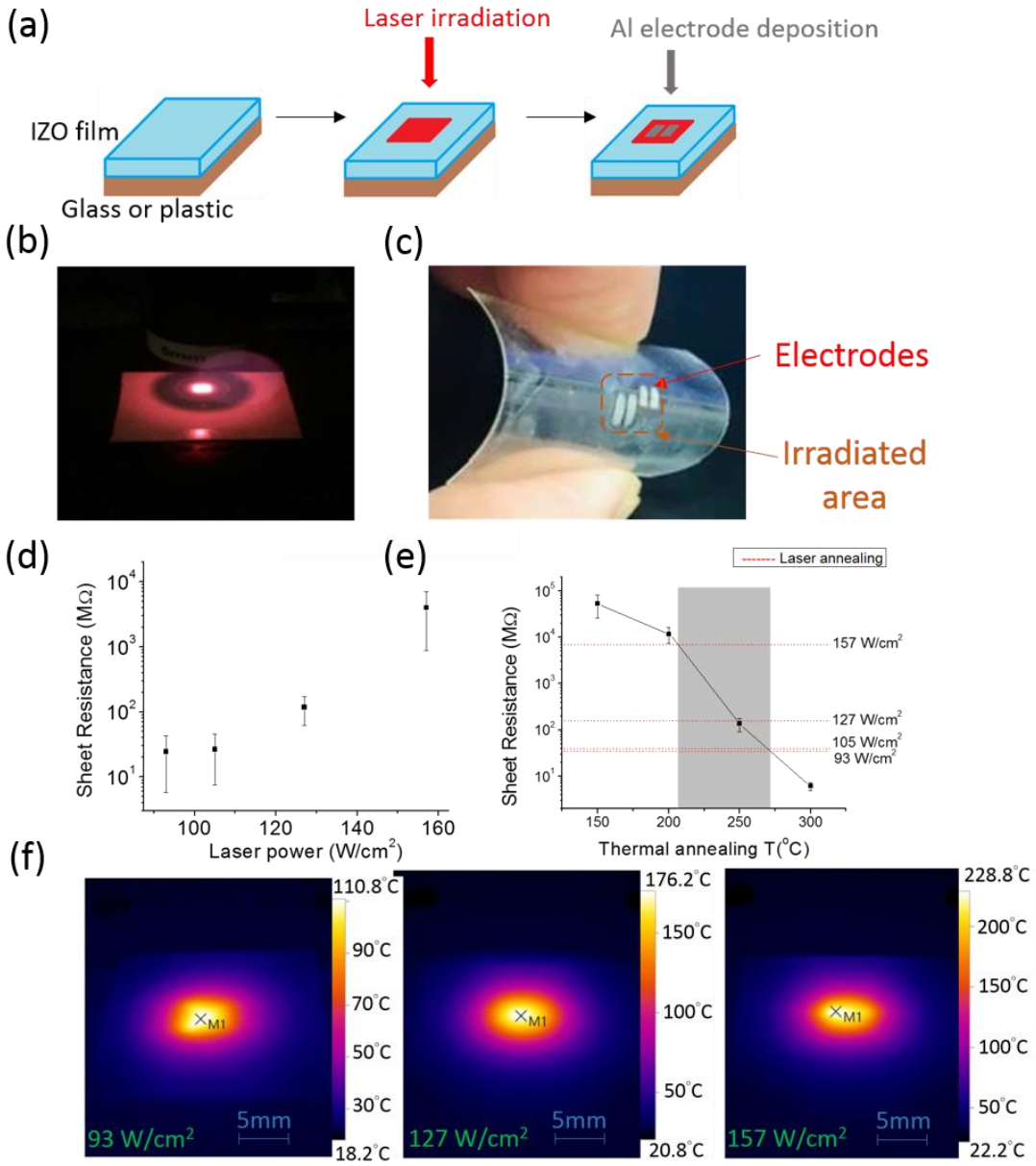

Figure 2. (a) Schematic of the fabrication of IZO chemoresistor. (b) Photograph of the sample during NIR laser irradiation. (c) Photograph of the IZO chemoresistor device with Al electrodes on PC substrate, depicting the device in a bent state. (d) Sheet resistance (R_s) of the IZO thin film cured by NIR laser (60-s irradiation) as a function of laser power. (e) Comparison of thermal and laser annealing for R_s values. (f) NIR photographs of temperatures measured by thermal imager for different NIR laser power.

Results and Discussion

As depicted in Figure 2a, the key-step of the fabrication process relies on a photothermal effect that is triggered by the NIR laser irradiation and facilitated by the addition of the NIR dye. The local temperature increase allowed the classical condensation reactions to occur in the film and convert the material into metal oxide, with noteworthy electrical properties, as shown later.

The irradiation conditions were thus expected to have a strong effect on the final material properties. To investigate the effect of NIR laser annealing, different power densities were tested. Figure 2d illustrates the sheet resistance (R_s) of the IZO chemoresistor with different laser doses. With 60-s irradiation, laser power was set to 93 W/cm^2, 105 W/cm^2, 127 W/cm^2, and 157 W/cm^2. Notably, it was not possible to use a laser power lower than 93 W/cm^2, because at a lower laser power, no stable electrical signal could be recorded. This was probably due to a low conversion of the material and the resulting high content of ionic species and solvent that can cause background electric signals and unstable device performance. As depicted in Figure 2d, when laser power was set to 93 W/cm^2 and 105 W/cm^2, the R_s remained almost constant at 25 MΩ. When laser power increased to 127 W/cm^2 and 157 W/cm^2, the R_s increased to 118 MΩ and 3950 MΩ, respectively.

We compared the R_s of the NIR-laser-annealed IZO film with the R_s of thermally annealed IZO film. Figure 1e demonstrates the R_s of IZO films with different thermal annealing conditions. Thermal annealing was applied using a furnace tube with the temperature set to 150°C, 200°C, 250°C, and 300°C for 1 h. As expected, when the annealing temperature increased, the R_s of the IZO film decreased, which confirmed the need for thermal curing to obtain suitable electrical properties. The R_s values of NIR-laser-annealed films are denoted by the red dashed lines in Figure 2e. The R_s of NIR-laser-annealed IZO films with laser power from 93 W/cm^2 to 157 W/cm^2 (60 s) were comparable to those of thermally annealed films with annealing temperature from 200–300°C (1 h). The 60 s laser irradiation time, however, was much shorter than the 1 h thermal annealing time. In addition, laser irradiation only generated local heating, whereas thermal annealing heated the whole substrate, and thus it cannot be applied to a plastic substrate. We observed that the proposed NIR laser annealing method was advantageous to the formation of the IZO chemoresistor on a plastic substrate as a flexible device. The flexible device performance is discussed later.

Figure 2f is the real-time thermal image taken by a thermal imager (Testo 875i - versatile) on samples with NIR laser annealing for 60 s. The images, recorded shortly after ceasing NIR irradiation, confirmed the local heating generated at the surface of

the samples. The laser powers of 93 W/cm^2, 127 W/cm^2, and 157 W/cm^2, generated maximum temperatures of 110.8°C, 176.2°C, and 228.8°C, respectively. The measured temperatures were in the same order of magnitude as those used for thermal curing.

To confirm the laser-induced modification of the IZO thin film, we used ATR-FTIR analysis. As evident in Figure 3a, both thermal and laser annealing showed a substantial reduction at the peak of approximately 1400 cm^{-1}. This peak can be ascribed to nitrate ions, indicating that the nitrate ions are removed during both laser and thermal treatments with a similar yield.[32] The reduction of the absorbance of the broad peak at 3500 cm^{-1} indicates that the OH are also consumed in both conditions, which is consistent with condensation reaction between metal-oxide species.

XPS analysis was also used to investigate the chemical changes induced by NIR laser and thermal treatment of the IZO films. As shown in previous works[33], condensation reaction of the sol-gel material thin film can be followed quantitatively by following the modification of the O 1s component. The original data are provided in supporting information S3, S4 and Table S1. The three peaks are 530.4 eV, standing for surface hydroxide and lattice hydroxide; 529.2 eV, standing for vacancies and lattice defect; and 528.6 eV standing for the metal-oxide bonding network.[33] We observed a slight difference in peak positions that may be ascribed to the charging

effect or the difference in morphology detected by AFM measurements (Figure 3e). The ratio between the intensity of the three specific peaks of thermal and laser annealing films are compared in Figures 3b and 3c. We expect that the thermal or laser annealing provokes the condensation of the sol-gel thin film, promoting the conversion of defects (surface and lattice hydroxides and defects) into metal oxide network. For thermal annealing (Figure 3b), we observed, as expected, the condensation reaction of the metal-oxide network, with further conversion of the hydroxide species to metal-oxide lattice species. With increasing temperature, the proportion of vacancy and lattice defects decreased, which accounts for the improvement of the electrical properties. In Figure 3c, the effect of the NIR laser is plotted. Metal-oxide lattice was 50%, 48%, and 49% for samples with laser powers of 93 W/cm^2, 107 W/cm^2, and 157 W/cm^2, respectively. Such metal-oxide lattice ratios are comparable to those of samples prepared under a 300°C thermal annealing condition (53%), as shown in Figure 3b. The finding of extremely similar metal-oxide lattice ratios for the laser-annealed samples also suggests that changing laser power from 93 W/cm^2 to 157 W/cm^2 does not substantially change the film composition. The XPS data are in agreement with the electrical properties presented in Figure 2, showing that the 60-s irradiation is efficient enough to generate the same effect in the thin film as thermal heating at 200°–300°C during 60 min.

Laser irradiation time is another critical parameter. With a fixed laser power of 93 W/cm^2, the irradiation time was tuned to 0 s, 30 s, 60 s, 90 s, and 120 s. The raw XPS analysis data are provided in supporting information. The ratio of hydroxide (530.4 eV) to the sum of the three peaks is plotted as a function of laser irradiation time, as shown in Figure 3d. This result suggests that a laser irradiation time of 60 s is sufficient to substantially remove the surface hydroxide defect. We also noticed that increasing irradiation time from 60 s to 120 s did not further improve the conductivity (data not shown), hence we chose 60 s as our optimal irradiation time.

To further investigate the reduction of conductivity with the increase of laser power, the film morphology was also studied by using AFM. The surface roughness of IZO film, as a function of laser power, is shown in Figure 3e. The AFM images of IZO film with the lowest laser power of 93 W/cm^2 and the highest laser power of 157 W/cm^2 are shown in Figures 3f and 3g, respectively. The AFM images of samples with laser power of 105 W/cm^2 and 127 W/cm^2 are shown in supporting information Figure S4. It can clearly be observed in Figure 3f that the IZO film with high laser power (i.e., 157 W/cm^2) exhibits a very rough morphology (roughness as high as 77 nm). In Figure 2d, with increased laser power, the film roughness increases considerably. The high roughness may be explained by the rapid heating on the IZO film during the laser irradiation, which causes fast evaporation of the solvent and

leads to the nonuniformity of the film. We therefore suggest that, as evident in Figure 2d, the degraded conductivity with high laser power is caused by the greatly increased film roughness. Notably, in Figure 3e, the surface roughness of the IZO film with low laser power is comparable to the roughness of the IZO film with 300°C thermal annealing for 1 h.

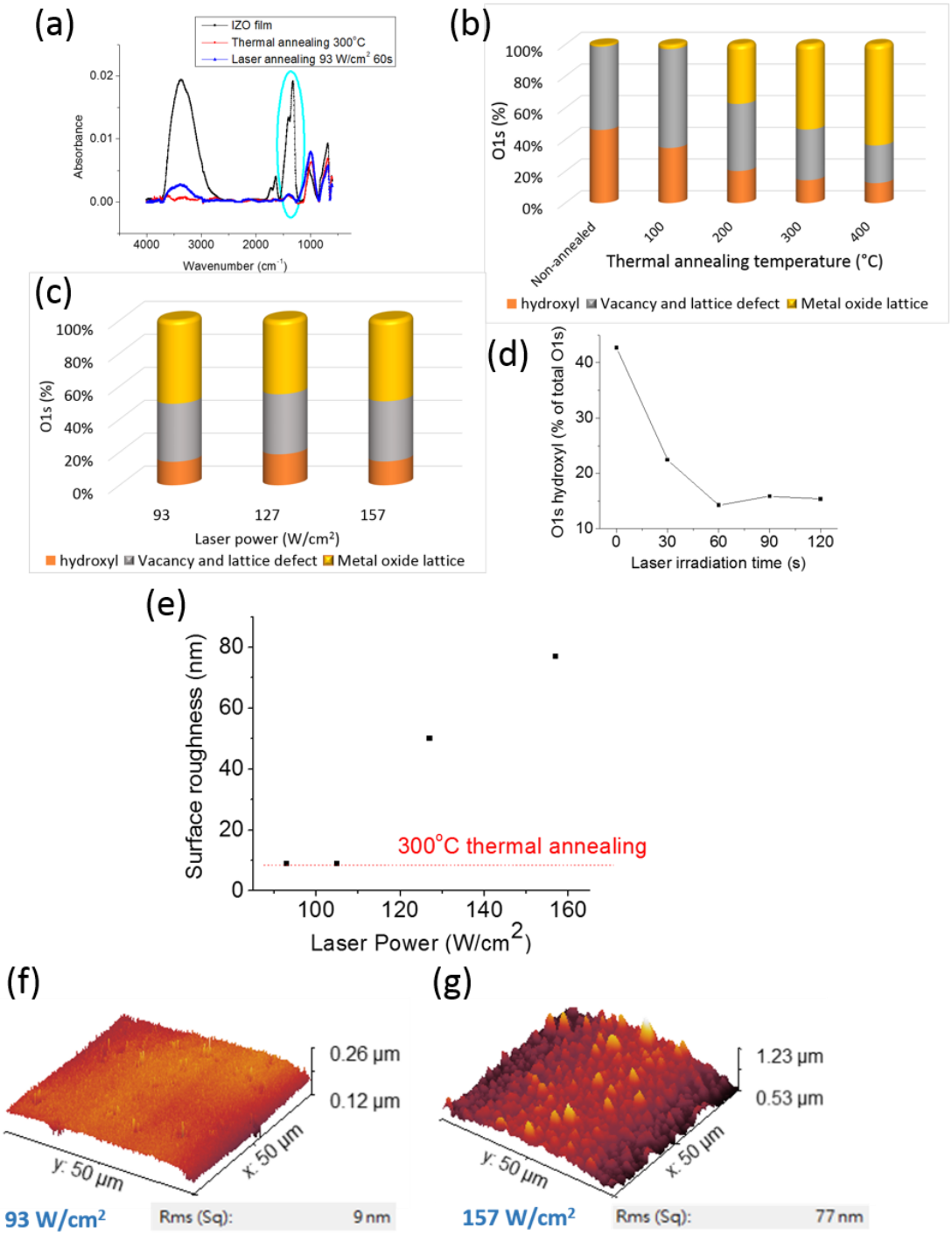

Figure 3. (a) ATR-FTIR analysis of the IZO thin film for laser and thermal annealing. The highlighted area corresponds to the removal of nitrate ions under both the thermal and laser annealing processes. (b), (c) Analysis of O1s peak from the XPS data for thermal and laser annealing, respectively. (b) shows the fluctuation of three main peaks, hydroxyl, vacancy and lattice defect, and metal-oxide lattice, for several temperatures. (c) shows the similar metal-oxide ratio of laser power at 93 W/cm^2, 127 W/cm^2, and 157 W/cm^2.

(d) Evolution of hydroxyl content with different laser irradiation times. (e) Surface roughness of IZO film as a function of laser power. The irradiation time was 60 s. (f), (g) AFM images to compare low (93 W/cm^2) and high (157 W/cm^2) laser power differences.

A notable characteristic of the NIR laser curing process is its compatibility with plastic substrates that cannot stand thermal curing. For this reason, devices on plastic substrates were fabricated and their electrical properties were evaluated. We successfully used the NIR laser annealing method on flexible substrates such as PE, PET, and PC without damaging the substrates, as shown in Figure S5. Thermal annealing at 200°C for 1 h caused obvious deformation of these substrates. For example, normally, PC begins to flow at temperatures above 150°C. Such temperatures are too low to form thermally annealed IZO film with suitable electrical properties.

IZO semiconducting thin films are known to be sensitive to gas, and this material can thus be used in a chemoresistor material. After verifying that the film composition and the sheet resistance of NIR-laser-annealed IZO film are as good as their thermal annealed counterparts, we investigated the sensor performance of the fabricated IZO film. For sensor application, we like to have a large enough output current (i.e. 10^{-8} ~ 10^{-6} A) at a low operation voltage (i.e. 5-10 volts) to avoid the noise in the electrical measurement system. Hence, samples with 157 W/cm^2 60 sec are not very suitable

due to the high resistance. For the following samples, if not particularly specified, the laser annealing condition is 127 W/cm^2 for 60 sec. We first noticed that the film's electrical response was very sensitive to humidity, hence humidity sensing results were demonstrated. Using the humidity control system described in the experimental section, we tested the real-time current change when modifying the humidity in the sensing chamber. As shown in Figure 4a, the relative humidity (RH) was variously 10%, 30%, 50%, and 60%. With increasing humidity, the current in the device elevated. Such an effect was also reported in prior works. Water molecules absorbed onto the surface of the metal oxide to form H^+ or H_3O^+ through a dissociation effect.[34,35] Then, H^+ or H_3O^+ ions hopped between adjacent hydroxyl groups to form the current. Increasing RH led to an increase of such hopping current.[34, 35] Notably, to have a consistent current response, 10% humidity was used as a background reference condition. With this controlled background reference, the IZO film delivered a stable response to humidity change, as shown in Figure 4a. The current response is defined as the average current when switching the humidity for 1 min and is plotted as a function of RH in Figure 4b. The small deviation verifies the function of humidity sensing. In future application, the reference 10% RH can be produced by flowing the background air through the NaOH tube as reported in our prior works.[5,8,18]

In the second step, we demonstrated that the IZO chemoresistor device can be integrated by laser annealing on flexible PC substrate, without any noticeable modification of the substrate properties (Figure 4c). We then illustrated the hydrogen sulfide gas-sensing performance of the device on a flexible substrate. With a fixed humidity of 62%, the proposed IZO chemoresistor had a very good response to hydrogen sulfide (H_2S) gas. It is noted that the humidity has to be fixed, otherwise the variation of humidity will cause an interference signal to the H_2S sensing. The method to control the humidity in the sensing system was introduced in the experimental section. The real-time current response to H_2S gas is illustrated in Figure 4d. In the orange regions, H_2S gas with 1000, 500, and 300 ppb concentration was injected into the sensing chamber for 30 s. The responding current drops were very fast and were reversible after removing the H_2S gas. The sensing response was defined as the current variation ratio, which is the current difference during the 30-s sensing period divided by the initial current level before injecting H_2S gas. When the sensing response is defined by using the current variation ratio, the response will not be affected by the absolute value of the current. [6,36] Hence, after the recovery period, even if the current level cannot reach its original value, the sensor delivers stable response to a fixed H_2S concentration. (Figure S6). The slight decrease of the background current signal during measurement may be due to the increased defect

density with continuous bias, which is known as the bias stress effect in oxide semiconductor devices [37]. Figure 4e demonstrates the calibration curve by plotting the sensing response as a function of H_2S concentration. For every H_2S concentration, three sensing responses were recorded to calculate the average and standard deviation. A linear dependence was obtained. As mentioned in Fig. 3(e), NIR laser intensity modulated the surface roughness. We compared the H_2S sensing responses by using the IZO films annealed by 93 W/cm^2 and 157 W/cm^2, with corresponding AFM images shown in Figs. 3(f) and 3(g), respectively. However, no significant difference was observed between the two sensors' responses (data not shown), indicating that the surface roughness is not the primary factor to control the H_2S sensing. In prior reports, when using SnO_2 or Cu-doped ZnO to detect H_2S, a current increase was observed upon exposure to H_2S with ppm-regime concentrations. [36, 38-40] Other recent reports[29-31, 41-44] for H_2S sensing are compared in Table S2. For H_2S sensing on flexible substrate, we are the first to deliver sensitivity in ppb-regime. The sensing mechanism, particularly at operating temperatures above 140°C, is mostly explained by the reaction between H_2S molecules and O^- or O_2^- to generate additional free electrons. The high temperature greatly enhances the adsorption activity of oxygen onto the surface of the metal-oxide semiconductor. The conversion rate of adsorbed molecular oxygen (O_2^-) to atomic oxygen ($2O^-$) is also increased at elevated

temperatures. The H_2S molecules then react with O^- or O_2^- to form SO_2 and free electrons. Hence, a current increase is obtained when detecting H_2S. However, in our work, we repeatedly observed a current drop when the NIR-annealed IZO chemoresistor was in contact with H_2S. When we reduced the RH in the sensing chamber to 30%, as shown by the red line in Figure 4e, the responses to H_2S were almost the same as those with RH of 62%. Such a humidity effect on gas sensing in IZO differs from prior reports. In previous works, a degraded CO or H_2S sensing response is observed when increasing the humidity. The elevated water absorption on the ZnO surface shields the reactive O^- or O_2^- sites and hence suppresses the response to H_2S gas.[22] In the current work, we observed a current reduction in IZO upon H_2S sensing at room temperature. In addition, the sensing capacity was not degraded by increasing the humidity. It is thus plausible that the H_2S detection of our sample does not rely on the reaction with O^- or O_2^-. The detailed mechanism, however, requires further investigation. In this work, we aimed to propose a new annealing method to realize flexible IZO on a plastic substrate and to deliver an ultrasensitive ppb-regime H_2S-sensing performance.

Finally, we evaluate sensing selectivity. Figure 4f shows the sensing response to ammonia (NH_3), acetone (denoted as ACE), nitrogen monoxide (NO), and hydrogen sulfide (H_2S) with a gas concentration of 1 ppm. We noticed that the proposed IZO

film was particularly sensitive to H_2S. The high sensitivity and selectivity to H_2S gas indicates that the NIR-laser-annealed IZO film is promising for application in industries or households for safety surveillance. As a preliminary test, we also compared the H_2S sensing response using a just-fabricated sensor (noted as Day 0) and a sensor stored at a food-storage-quality nitrogen bag for 2 days (noted as Day 2) in Fig. S7 in supporting information. There is no much difference between the Day 0 and Day 2 data. Also, within 2 hrs, the sensor delivers repeated sensing results even when the background current decreases due to the continuous bias effect (not shown). In future, more studies will be conducted to investigate the optimal storage condition to obtain a good enough shelf-lifetime for real applications.

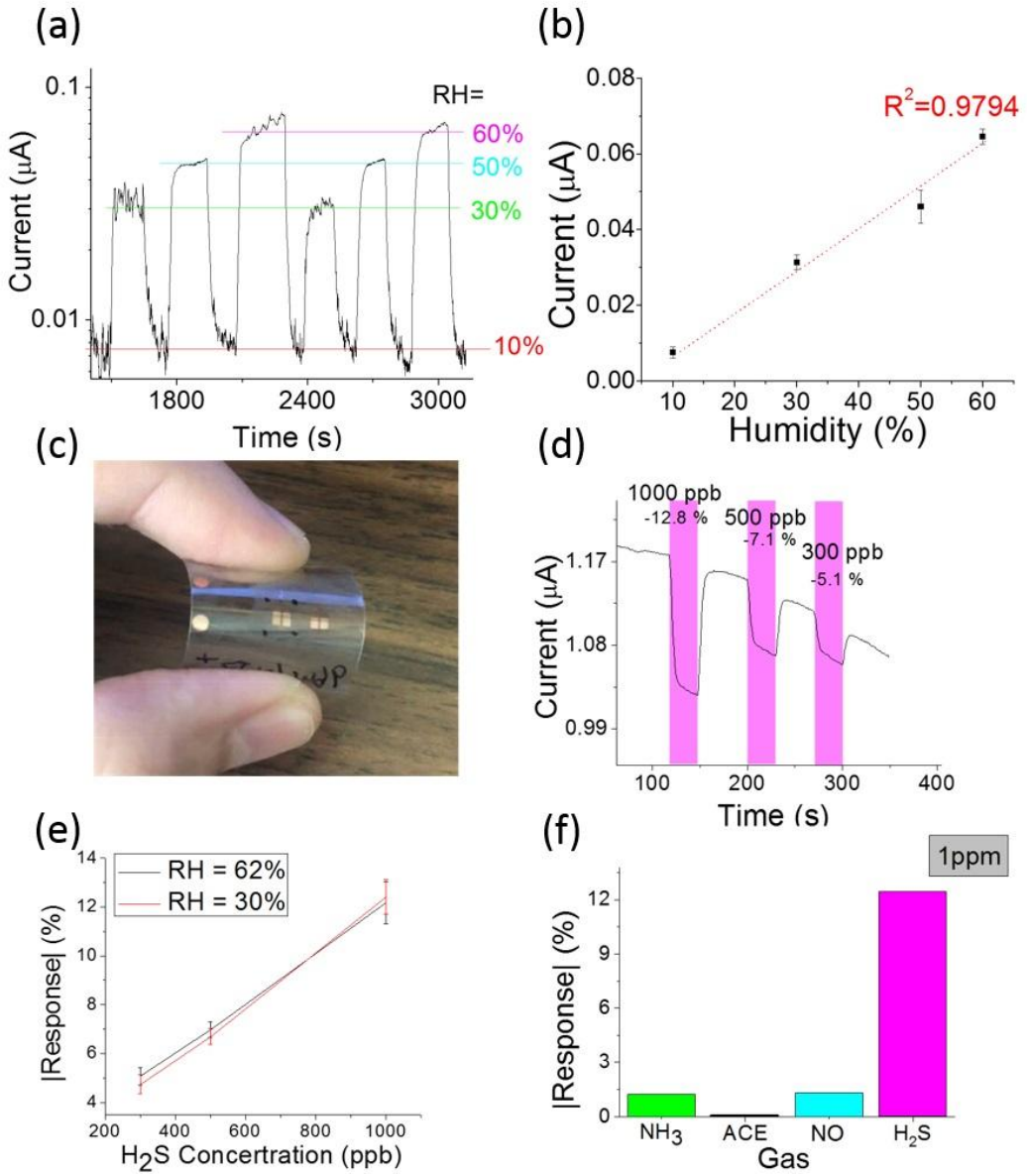

Figure 4. (a) Current response of NIR laser-annealed device. The NIR laser irradiation power was 127 W/cm^2 for 60 s on PC substrate. The operation voltage was 10 volts. (b) Calibration curve of NIR laser-annealed humidity sensor. With the change of humidity, we extracted and calculated the first 120 s of current data once it became stable. (c) Photograph of NIR-laser-annealed IZO chemoresistor on a bendable PC substrate. (d) The real-time current response and gas response of NIR-laser-annealed IZO chemoresistor when injecting H_2S gas with different concentrations. The operation voltage was 5 volts. The NIR laser power density was 127 W/cm^2 for 60 s. (e) Calibration curves of NIR-laser-annealed IZO chemoresistor on PC substrate at RH = 62% and RH = 30%. The NIR laser power density was 127 W/cm^2 for 60 s. Three independent experiments were conducted to

calculate the average and the standard deviation. (f) The comparison of sensing response to 1-ppm ammonia, acetone, nitric oxide, and hydrogen sulfide.

Conclusion

We demonstrated a new 808-nm NIR laser-based method to treat sol–gel IZO film that has a low-cost and fast annealing time. The performance of the laser-annealed device is comparable with that of a thermally annealed device with an annealing temperature above 200°C. The short laser irradiation time and the local heating phenomenon make the NIR laser suitable for fabrication on flexible substrates such as PC. The XPS analysis confirmed that the proposed NIR laser annealing method provides a suitable metal-oxide network for electric conduction. The NIR-laser-annealed IZO film was then used as a humidity sensor and hydrogen sulfide sensor. For humidity sensing, compared with the reference humidity, the IZO film delivered a stable sensing response to RH, varying from 10% to 60%. Then, with a fixed humidity, the IZO film exhibited an extremely sensitive response to H_2S, ranging from 300 to 1000 ppb. The sensing mechanism does not rely on the interaction between H_2S and the absorptive of oxygen (O^- or O_2^-), which is only present at high temperatures. As a result, in our work, ppb-regime H_2S sensing can be realized at room temperature on a bendable substrate. The H_2S sensing selectivity among ammonia, nitric monoxide, carbon monoxide, and acetone is also extremely

favorable. Preliminary stability test on the proposed H_2S sensor revealed that the sensor delivered almost unchanged sensing response after being stored in a simple food-storage-quality nitrogen bag for 2 days. More investigation on long term stability and storage condition will be done in future work. The proposed low-cost bendable NIR-laser-annealed IZO chemoresistor is promising for use in wearable devices to detect environmental humidity or to give an alert of dangerous hydrogen sulfide levels.

Acknowledgements

The authors like to thank Philippe Fioux and Banjamin Leuschel for their assistance to run XPS and AFM experiments. This work was supported by funding from Agence Nationale pour la Recherche (Project PHOTOMOC, ANR-14-CE26-0039 and Project NIRTRONIC, ANR-18-CE24-0028), Institut Carnot MICA (project SENSORTEX) and Ministry of Science and Technology, Taiwan (Projects 108-2923-E-009-002-MY3 and 108-2221-E-009-114-).

References

[1] Chatterjee, S. G.; Chatterjee, S.; Ray, A. K.; Chakraborty, A. K. (2015). Graphene–metal oxide nanohybrids for toxic gas sensor: a review. *Sensors and Actuators B: Chemical*, *221*, 1170-1181.

[2] Liu, W.; Liu, Y. Y.; Do, J. S.; Li, J. (2016). Highly sensitive room temperature ammonia gas sensor based on Ir-doped Pt porous ceramic electrodes. *Applied Surface Science*, *390*, 929-935.

[3] Konvalina, G.; Haick, H. (2014). Sensors for breath testing: from nanomaterials to comprehensive disease detection. *Accounts of chemical research*, *47*(1), 66-76.

[4] Machado, R. F.; Laskowski, D.; Deffenderfer, O.; Burch, T.; Zheng, S.; Mazzone, P. J.; Mekhail T.; Jennings C.; Stoller K. James; Pyle J.; Duncan, J. (2005). Detection of lung cancer by sensor array analyses of exhaled breath. *American journal of respiratory and critical care medicine*, *171*(11), 1286-1291.

[5] Chuang, M. Y.; Chen, C. C.; Zan, H. W.; Meng, H. F.; Lu, C. J. (2017). Organic gas sensor with an improved lifetime for detecting breath ammonia in

hemodialysis patients. *ACS sensors*, *2*(12), 1788-1795.

[6] Singh, P.; Hu, L. L.; Zan, H. W.; Tseng, T. Y. (2019). Highly sensitive nitric oxide gas sensor based on ZnO-nanorods vertical resistor operated at room temperature. *Nanotechnology*, *30*(9), 095501.

[7] Timmer, B.; Olthuis, W.; Van Den Berg, A. (2005). Ammonia sensors and their applications—a review. *Sensors and Actuators B: Chemical*, *107*(2), 666-677.

[8] Chang, L. Y.; Chuang, M. Y.; Zan, H. W.; Meng, H. F.; Lu, C. J.; Yeh, P. H.; Chen, J. N. (2017). One-minute fish freshness evaluation by testing the volatile amine gas with an ultrasensitive porous-electrode-capped organic gas sensor system. *ACS sensors*, *2*(4), 531-539.

[9] Park, S.; Kim, K. H.; Jo, J. W.; Sung, S.; Kim, K. T.; Lee, W. J.; Kim J.; Kim H. J.; Yi G. R.; Kim Y. H.; Yoon, M. H. (2015). In-Depth Studies on Rapid Photochemical Activation of Various Sol–Gel Metal Oxide Films for Flexible Transparent Electronics. *Advanced Functional Materials*, *25*(19), 2807-2815.

[10] Rieu, M.; Camara, M.; Tournier, G.; Viricelle, J. P.; Pijolat, C.; de Rooij, N. F.; Briand, D. (2016). Fully inkjet printed SnO2 gas sensor on plastic substrate. *Sensors and Actuators B: Chemical*, *236*, 1091-1097.

[11] Jo, J. W.; Kim, J.; Kim, K. T.; Kang, J. G.; Kim, M. G.; Kim, K. H.; Ko H.; Kim Y. H.; Park, S. K. (2015). Highly Stable and Imperceptible Electronics Utilizing Photoactivated Heterogeneous Sol-Gel Metal–Oxide Dielectrics and Semiconductors. *Advanced Materials*, *27*(7), 1182-1188.

[12] Yao, M. S.; Tang, W. X.; Wang, G. E.; Nath, B.; Xu, G. (2016). MOF Thin Film-Coated Metal Oxide Nanowire Array: Significantly Improved Chemiresistor Sensor Performance. *Advanced Materials*, *28*(26), 5229-5234.

[13] Wang, F.; Li, H.; Yuan, Z.; Sun, Y.; Chang, F.; Deng, H.; Xie L.; Li, H. (2016). A highly sensitive gas sensor based on CuO nanoparticles synthetized via a sol–gel method. *RSC advances*, *6*(83), 79343-79349.

[14] Mirzaei, A.; Janghorban, K.; Hashemi, B.; Bonyani, M.; Leonardi, S. G.; Neri, G. (2016). Highly stable and selective ethanol sensor based on α-Fe2O3 nanoparticles prepared by Pechini sol–gel method. *Ceramics International*, *42*(5), 6136-6144.

[15] Kim, J. W.; Porte, Y.; Ko, K. Y.; Kim, H.; Myoung, J. M. (2017). Micropatternable double-faced ZnO nanoflowers for flexible gas sensor. *ACS applied materials & interfaces*, *9*(38), 32876-32886.

[16] Zheng, Z. Q.; Yao, J. D.; Wang, B.; Yang, G. W. (2015). Light-controlling, flexible and transparent ethanol gas sensor based on ZnO nanoparticles for

wearable devices. *Scientific reports*, *5*, 11070.

[17] Li, S.; Lin, P.; Zhao, L.; Wang, C.; Liu, D.; Liu, F.; Sun P.; Liang X.; Liu F.; Yan X.; Gao, Y. (2018). The room temperature gas sensor based on Polyaniline@ flower-like WO3 nanocomposites and flexible PET substrate for NH3 detection. *Sensors and Actuators B: Chemical*, *259*, 505-513.

[18] Zan, H. W.; Li, C. H.; Yeh, C. C.; Dai, M. Z.; Meng, H. F.; Tsai, C. C. (2011). Room-temperature-operated sensitive hybrid gas sensor based on amorphous indium gallium zinc oxide thin-film transistors. *Applied Physics Letters*, *98*(25), 253503.

[19] Jaisutti, R.; Kim, J.; Park, S. K.; Kim, Y. H. (2016). Low-temperature photochemically activated amorphous indium-gallium-zinc oxide for highly stable room-temperature gas sensors. *ACS applied materials & interfaces*, *8*(31), 20192-20199.

[20] Leuschel, B.; Gwiazda, A.; Heni, W.; Diot, F.; Yu, S. Y.; Bidaud, C.; Vonna L.; Ponche A.; Haidara H.; Soppera, O. (2018). Deep-UV photoinduced chemical patterning at the micro-and nanoscale for directed self-assembly. *Scientific reports*, *8*(1), 1-15.

[21] Park, G. C.; Hwang, S. M.; Lee, S. M.; Choi, J. H.; Song, K. M.; Kim, H. Y.; Kim H. S.; Eum S. J.; Jung S. B.; Lim J. H.; Joo, J. (2015). Hydrothermally

grown in-doped ZnO nanorods on p-GaN films for color-tunable heterojunction light-emitting-diodes. *Scientific reports*, *5*, 10410.

[22] Stehlin, F.; Wieder, F.; Spangenberg, A.; Le Meins, J. M.; Soppera, O. (2014). Room-temperature preparation of metal-oxide nanostructures by DUV lithography from metal-oxo clusters. *Journal of Materials Chemistry C*, *2*(2), 277-285.

[23] Lin, H. C.; Stehlin, F.; Soppera, O.; Zan, H. W.; Li, C. H.; Wieder, F.; Ponche A.; Berling D.; Yeh B. H.; Wang, K. H. (2015). Deep ultraviolet laser direct write for patterning sol-gel InGaZnO semiconducting micro/nanowires and improving field-effect mobility. *Scientific reports*, *5*(1), 1-11.

[24] Yeh, C. C.; Liu, H. C.; Heni, W.; Berling, D.; Zan, H. W.; Soppera, O. (2017). Chemical and structural investigation of zinc-oxo cluster photoresists for DUV lithography. *Journal of Materials Chemistry C*, *5*(10), 2611-2619.

[25] Breaban, F.; Coutouly, J. F.; Braud, F.; Deprez, P. (2015). Nd: YAG Laser Beam-Material Interactions for Marking and Engraving: Application to Alumina and Granite. *Lasers in Engineering (Old City Publishing)*, *30*.

[26] Noor, Y. M.; Tam, S. C.; Lim, L. E. N.; Jana, S. (1994). A review of the Nd: YAG laser marking of plastic and ceramic IC packages. *Journal of Materials Processing Technology*, *42*(1), 95-133.

[27] Ezra, N.; Arshanapalli, A.; Bednarek, R.; Akaishi, S.; Somani, A. K. (2016). The microsecond 1064 nm Nd: YAG laser as an adjunct to improving surgical scars following Mohs micrographic surgery. *Journal of Cosmetic and Laser Therapy*, *18*(4), 225-229.

[28] Chang, P. Y.; Bruntz, A.; Vidal, L.; Vetter, P. A.; Roudot, P.; Bua, L.; Ortiz J.; Zan H. W.; Soppera, O. (2019). Laser Polymer Tattooing: A Versatile Method for Permanent Marking on Polymer Surfaces. *Macromolecular Materials and Engineering*, *304*(12), 1900402.

[29] Asad, M.; Sheikhi, M. H.; Pourfath, M.; Moradi, M. (2015). High sensitive and selective flexible H2S gas sensors based on Cu nanoparticle decorated SWCNTs. *Sensors and Actuators B: Chemical*, *210*, 1-8.

[30] Joshi, N.; Saxena, V.; Singh, A.; Koiry, S. P.; Debnath, A. K.; Chehimi, M. M., Aswal D. K.; Gupta, S. K. (2014). Flexible H2S sensor based on gold modified polycarbazole films. *Sensors and Actuators B: Chemical*, *200*, 227-234.

[31] Mousavi, S.; Kang, K.; Park, J.; Park, I. (2016). A room temperature hydrogen sulfide gas sensor based on electrospun polyaniline–polyethylene oxide nanofibers directly written on flexible substrates. *RSC advances*, *6*(106), 104131-104138.

[32] Miller, F. A.; Wilkins, C. H. (1952). Infrared spectra and characteristic frequencies of inorganic ions. *Analytical chemistry*, *24*(8), 1253-1294.

[33] Lin, H. C.; Stehlin, F.; Soppera, O.; Zan, H. W.; Li, C. H.; Wieder, F.; Ponche A.; Berling D.; Yeh B. H.; Wang, K. H. (2015). Deep ultraviolet laser direct write for patterning sol-gel InGaZnO semiconducting micro/nanowires and improving field-effect mobility. *Scientific reports*, *5*(1), 1-11.

[34] Traversa, E. (1995). Ceramic sensors for humidity detection: the state-of-the-art and future developments. *Sensors and Actuators B: Chemical*, *23*(2-3), 135-156.

[35] Wang, C.; Yin, L.; Zhang, L.; Xiang, D.; Gao, R. (2010). Metal oxide gas sensors: sensitivity and influencing factors. *Sensors*, *10*(3), 2088-2106.

[36] Verma, M. K.; Gupta, V. (2012). A highly sensitive SnO2–CuO multilayered sensor structure for detection of H2S gas. *Sensors and Actuators B: Chemical*, *166*, 378-385.

[37] Park, H.; Nam, Y.; Jin, J.; Bae, B. S. (2014). Improvement of bias stability of oxyanion-incorporated aqueous sol–gel processed indium zinc oxide TFTs. *Journal of Materials Chemistry C*, *2*(30), 5998-6003.

[38] Shewale, P. S.; Patil, V. B.; Shin, S. W.; Kim, J. H.; Uplane, M. D. (2013). H2S gas sensing properties of nanocrystalline Cu-doped ZnO thin films prepared

by advanced spray pyrolysis. *Sensors and Actuators B: Chemical*, *186*, 226-234.

[39] Manorama, S.; Devi, G. S.; Rao, V. J. (1994). Hydrogen sulfide sensor based on tin oxide deposited by spray pyrolysis and microwave plasma chemical vapor deposition. *Applied physics letters*, *64*(23), 3163-3165.

[40] Gong, J.; Chen, Q.; Lian, M. R.; Liu, N. C.; Stevenson, R.G.; Adami, F. (2006). Micromachined nanocrystalline silver doped SnO2 H2S sensor. *Sensors and Actuators B: Chemical*, *114*(1), 32-39.

[41] Li, Z.; Wang, N.; Lin, Z.; Wang, J.; Liu, W.; Sun, K.; Fu Y. Q.; Wang, Z. (2016). Room-temperature high-performance H2S sensor based on porous CuO nanosheets prepared by hydrothermal method. *ACS applied materials & interfaces*, *8*(32), 20962-20968.

[42] Wang, Y.; Liu, B.; Xiao, S.; Wang, X.; Sun, L.; Li, H.; Xie W.; Li Q.; Zhang Q.; Wang, T. (2016). Low-temperature H2S detection with hierarchical Cr-doped WO3 microspheres. *ACS applied materials & interfaces*, *8*(15), 9674-9683.

[43] Tian, K.; Wang, X. X.; Yu, Z. Y.; Li, H. Y.; Guo, X. (2017). Hierarchical and hollow Fe2O3 nanoboxes derived from metal–organic frameworks with excellent sensitivity to H2S. *ACS applied materials & interfaces*, *9*(35),

29669-29676.

[44] Kim, M. H.; Jang, J. S.; Koo, W. T.; Choi, S. J.; Kim, S. J.; Kim, D. H.; Kim, I. D. (2018). Bimodally porous WO3 microbelts functionalized with Pt catalysts for selective H2S sensors. *ACS applied materials & interfaces*, *10*(24), 20643-20651.

TOC Graphic

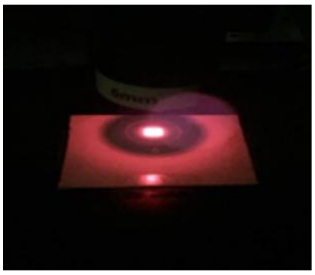

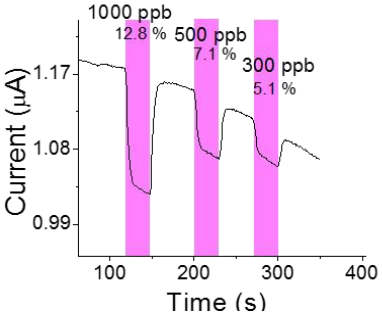
1000 ppb
12.8 %
500 ppb
7.1 %
300 ppb
5.1 %
Current (μA)
1.17
1.08
0.99
100
200
300
400
Time (s)